Eur. Phys. J. B **14**, 251–261 (2000)

**THE EUROPEAN PHYSICAL JOURNAL B**

EDP Sciences


# Analysis of the first electron-removal states of $Ba_2Cu_3O_4Cl_2$ using polarization dependent angle-resolved photoelectron spectroscopy

S. Haffner[1,a], M. Knupfer[1,b], S.R. Krishnakumar[1,c], K. Ruck[1], G. Krabbes[1], M.S. Golden[1], J. Fink[1], and R.L. Johnson[2]

[1] Institut für Festkörper- und Werkstofforschung Dresden, P.O. Box 270016, 01171 Dresden, Germany
[2] Institut für Experimentalphysik, Universität Hamburg, Luruper Chaussee 149, 22761 Hamburg, Germany

Received 19 March 1999 and Received in final form 15 August 1999

**Abstract.** The first electron-removal states of the layered cuprate $Ba_2Cu_3O_4Cl_2$ were measured using angle-resolved photoelectron spectroscopy. The symmetry and energy-momentum relations of the lowest-lying states were determined and interpreted in terms of the motion of a single hole in the two different planar Cu-O subsystems of the $Cu_3O_4$ plane. One subsystem is antiferromagnetic as in the undoped parent compounds of the high-temperature superconductors and the other is paramagnetic and corresponds to the strongly overdoped case. The data are compared to theoretical results on hole dynamics in two-dimensional antiferromagnetic or paramagnetic spin backgrounds. The lineshape, symmetry and dispersion of the first electron-removal states of $Ba_2Cu_3O_4Cl_2$ can be described in terms of Zhang-Rice singlets within a single band model. The photohole lifetime in the paramagnetic subsystem of the $Cu_3O_4$ plane is much smaller than with an antiferromagnetic spin background.

**PACS.** 74.72.Jt Other cuprates – 79.60.-i Photoemission and photoelectron spectra – 71.27.+a Strongly correlated electron systems; heavy fermions

## 1 Introduction

Recently, angle-resolved photoelectron spectroscopy (ARPES) has played a key role in revealling the electronic structure of the high-temperature superconductors (HTSC's). ARPES measurements have proven the existence of Fermi surfaces that enclose a significant fraction of the Brillouin zone (BZ) in the normal state in accordance with band-structure calculations [1]. Further successes include the observation of anisotropic energy gaps in the superconducting state [2], and the existence of a pseudogap in the underdoped region of the phase diagram [3]. Despite these impressive results many questions remain unanswered. One question concerns the influence of the magnetic background on the electronic structure of the HTSC's, *i.e.* the evolution of the electronic structure upon doping from an insulator with long-range antiferromagnetic order *via* "strange" metallic behavior at optimal doping to normal paramagnetic metallic behavior in the strongly overdoped regime. Although there is no long-range magnetic order outside the antiferromagnetic insulating region of the phase diagram, it seems that the short-range antiferromagnetic correlations still influence the electronic structure. Systematic studies of the influence of the magnetic background on the electronic structure of the HTSC's with ARPES are hindered by the need for high sample surface quality. Most of the work has been done on BSCCO samples near optimal doping and ARPES data from underdoped or strongly overdoped HTSC samples have only become available recently [3,4]. No ARPES data from the undoped parent compounds of the HTSC's (*e.g.* $La_2CuO_4$) are available.

The copper oxychlorides $Sr_2CuO_2Cl_2$ and $Ba_2Cu_3$-$O_4Cl_2$ present an alternative to the undoped parent compounds of the HTSC's. They are closely related to the HTSC's in that they are layered compounds isostructural with the high temperature phase of $La_2CuO_4$ with Cu-O planes as fundamental building blocks. Further similarities are the two-dimensional character of their low-lying electronic states [5], which are dominated by contributions from Cu $3d_{x^2-y^2}$ and O $2p_{x,y}$ orbitals, and that they are antiferromagnetic insulators [6–8]. Neither a superconducting, nor even a metallic phase have been found in these systems up to now. A major difference between $Sr_2CuO_2Cl_2$ and $Ba_2Cu_3O_4Cl_2$ is the stoichiometry of the Cu-O planes: $Sr_2CuO_2Cl_2$ posseses $CuO_2$ planes as in the HTSC's, while

[a] *Present address*: Physical Sciences Laboratory, 3725 Schneider Drive, Stoughton, WI 53598-3098, USA
[b] e-mail: mknupfer@ifw-dresden.de
[c] *Present address*: Solid State and Structural Chemistry Unit, Indian Institute of Science, Bangalore 560 012, India

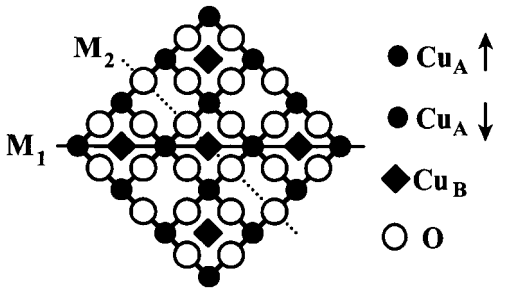


**Fig. 1.** Sketch of a $Cu_3O_4$ plane. The solid line designated as $M_1$ is a mirror plane of the $Cu_3O_4$ plane including the antiferromagnetic spin order (spin up: black circle, spin down: grey circle) in the $Cu_A$-O subsystem while the dotted line denoted by $M_2$ is a mirror plane of the geometrical structure alone.

$Ba_2Cu_3O_4Cl_2$ contains $Cu_3O_4$ planes (Fig. 1). In contrast to $CuO_2$ planes, $Cu_3O_4$ planes have two inequivalent copper sites: two thirds of the Cu atoms ($Cu_A$) occupy the Cu sites of the familiar $CuO_2$ plane while one third of the Cu atoms ($Cu_B$) reside in the center of every second mesh of the $CuO_2$ plane. $Ba_2Cu_3O_4Cl_2$ exhibits interesting magnetic properties which are directly related to the existence of two different Cu sublattices. Two antiferromagnetic transition temperatures have been measured: the first at $\sim$ 330 K [7,8] is comparable to the the Néel temperatures of $Sr_2CuO_2Cl_2$ ($T_N = 250$ K) [6]) and other undoped cuprates and is ascribed to antiferromagnetic ordering of the $Cu_A$ sub-lattice. The second transition is at 30 K for $Ba_2Cu_3O_4Cl_2$ [7,8] and marks the onset of antiferromagnetic ordering in the $Cu_B$ subsystem.

$Ba_2Cu_3O_4Cl_2$ and $Sr_2CuO_2Cl_2$ are interesting models for studying the electronic structure of two-dimensional correlated electron systems and aspects of high-temperature superconductivity. In a photoemission experiment hole doping occurs due to the photoionization process, which enables the dynamics of a single hole moving in a Cu-O plane to be studied [9–11]. This problem has been dealt with extensively in the literature of the theory of correlated electrons in the past few years [12].

$Ba_2Cu_3O_4Cl_2$ offers the exciting possibility of measuring the dispersion of a single hole moving in an antiferromagnetic ($Cu_A$-O subsystem) and a paramagnetic ($Cu_B$-O subsystem) background in a single room temperature photoemission experiment. ARPES data have been reported from $\Gamma$ to ($\pi$, 0) and from $\Gamma$ to ($\pi$, $\pi$) [13–15] which correspond to the low- and high-doping (strongly overdoped) limit of a Cu-O plane concerning the magnetic background. In this paper, an extended data set recorded at 20 eV photon energy with higher angular resolution is presented. We find that spectral features related to holes in the $Cu_B$-O subsystem are better developed at 20 eV than at 35 eV photon energy as used in references [13] and [14]. The data allow comprehensive tests of the current theoretical results on the dynamics of a single hole in two-dimensional antiferromagnetic or paramagnetic spin backgrounds.

## 2 Experimental

The ARPES measurements were performed at room temperature using linearly polarized 20 eV photons at beamline F2.2 in the Hamburg Synchrotron Radiation Laboratory (HASYLAB). The photoelectron spectrometer used was a Vacuum Generators ADES 400 spectrometer which was equipped with a 50 mm mean radius 150° sector hemispherical electron analyzer mounted on a two-axis goniometer. The angular resolution is ±1° which gives a momentum resolution of $\pm 0.03$ Å$^{-1}$ for the states of lowest binding energy, which corresponds to 10% of the distance between $\Gamma$ and ($\pi$, 0). With a pass energy of 5 eV the overall energy resolution was 150 meV. The spectra were recorded near normal-incidence, with the angle between the Poynting vector of the synchrotron radiation and the sample surface normal being 20°. This means that the electric field vector is nearly parallel to the sample surface, so states derived from in-plane orbitals dominate the photoelectron spectra. The base pressure of the analyzer chamber was $3 \times 10^{-11}$ mbar. The $Ba_2Cu_3O_4Cl_2$ single crystals were grown from the melt, their typical dimensions being $3 \times 3 \times 0.5$ mm. The crystals were mounted on the sample holders with conducting epoxy and their orientation was established *ex-situ* by X-ray diffraction. Prior to the ARPES measurements, a clean crystal sample surface parallel to the $Cu_3O_4$ planes was prepared in ultra-high vacuum by knocking off a cantilever glued on top of the sample. The spectra are normalized with respect to the ring current. To eliminate energy shifts due to sample charging reference spectra were measured with different photon fluxes. The absolute binding energy scale was fixed by comparison with the corresponding spectra in reference [13].

## 3 Results and discussion

This section is organized as follows: first, our approach to data analysis is explained. Then in the second part, the first electron-removal states taken along the lines $\Gamma$ to ($\pi$, 0) and $\Gamma$ to ($\pi$, $\pi$) as well as along the edges of the BZ and antiferromagnetic BZ are presented and their polarization dependence is discussed. Next, the origin of the two dispersive components observed in the first electron-removal states of $Ba_2Cu_3O_4Cl_2$ is discussed and their **k**-dependent energy variation is deduced. Finally, the ARPES data are compared to the results of theoretical models of the dynamics of a single hole in a two-dimensional antiferromagnetic or paramagnetic spin background and to the situation in $Sr_2CuO_2Cl_2$.

### 3.1 Data analysis

In recording an angle-resolved photoelectron spectrum, one measures the number of photoelectrons as a function of their kinetic energy (energy distribution curve (EDC)) with the photoelectron momentum as parameter. An EDC

shows the electron-removal excitation spectrum of the interacting electron system and in the sudden approximation the photoemission intensity is directly proportional to the matrix-element weighted spectral function. The spectral function itself is directly related to the imaginary part of the one-electron Green's function [16]. If the excitation spectrum of the interacting electron system is not too different from that of an interaction-free system, one can map the interacting electron system onto a system of weakly interacting QP's having finite lifetimes. The interaction is packed into the complex self-energy whose real part describes the renormalization of the QP energy with respect to the non-interacting electron system while the imaginary part accounts for the finite lifetime of the QP. In the QP approximation, the imaginary part of the self energy is much smaller than the renormalized QP energy [17]. A QP is thus visible as a Lorentzian peak in an EDC whose position determines the QP binding energy. In this work the dispersion of the first electron-removal states is analyzed using the QP hypothesis *i.e.* by fitting with Lorentzian functions which are convoluted by Gaussians to account for the analyzer energy resolution (resulting in a Voigt function) to the spectral intensity.

The first electron-removal states sit on a background of contributions from states at higher binding energies which can be subtracted before the positions of the first electron-removal states are deduced from the EDC's. As in reference [18], the influence of the higher lying states is represented by a Gaussian which has been fitted to the low binding energy flank of the spectral intensity related to the higher lying states. Contributions due to secondary electrons have been neglected as they should be negligibly small at the energies of the first electron-removal states [19]. Since we want to gain information about the dispersion of the lowest lying states (which are electronically two-dimensional), it is sufficient to know their momentum component parallel to the sample surface (parallel to the $Cu_3O_4$ planes). The parallel momentum in the sample is equal to the photoelectron momentum component parallel to the sample surface which is given by $\mathbf{k}_{||} = 0.512\,\text{Å}^{-1}\sqrt{E_{\text{kin}}[\text{eV}]}(\sin\theta\cos\phi\,\mathbf{k_x} + \sin\theta\sin\phi\,\mathbf{k_y})$ with ($\phi$, $\theta$) being the azimuthal and polar angles with respect to the sample surface normal and $E_{\text{kin}}$ is the kinetic energy of the photoelectrons. By varying the polar and azimuthal angles the energy of the lowest lying states as a function of their momentum vector, *i.e.* their dispersion relation, can be determined and compared to the results of model calculations.

The data are analyzed in terms of the BZ of the $Cu_3O_4$ plane, because the first electron-removal states are derived solely from the Cu $3d_{x^2-y^2}$ and O $2p_{x,y}$ orbitals in this plane. Figure 2 shows the region of **k**-space where EDC's have been recorded; the measured points are marked and the diameter of the filled circles indicates the **k**-resolution. The coordinates of the first BZ of the $Cu_3O_4$ plane of $Ba_2Cu_3O_4Cl_2$ are given. The $Cu_{A,B}$-O bonds are directed at an angle of 45° to the ($\pi$, 0) direction in **k**-space.

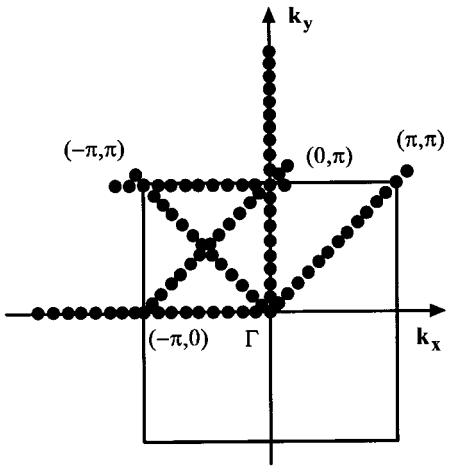


**Fig. 2.** A map of the locations in **k**-space at which EDC's have been recorded. The first BZ of the $Cu_3O_4$ plane of $Ba_2Cu_3O_4Cl_2$ is used as the unit cell of the reciprocal space and the labels are in units of the inverse lattice constant of the $Cu_3O_4$ plane.

### 3.2 The first electron removal states of $Ba_2Cu_3O_4Cl_2$ – polarization dependence

First we discuss the polarization dependence of the ARPES spectra along the lines $\Gamma$ to (0, $\pi$) and $\Gamma$ to ($\pi$, $\pi$). Figures 3a and 3b show the first electron-removal states of $Ba_2Cu_3O_4Cl_2$ scanned along the lines $\Gamma$ to (0, $\pi$) and $\Gamma$ to ($-\pi$, 0), respectively. The sample was oriented such that the analyzer has to be moved in a horizontal/vertical plane in order to select photoelectron momenta along the ($-\pi$, 0)/(0, $\pi$) directions in reciprocal space. It is evident from Figures 3a and 3b that there is a marked difference between the first electron-removal states measured in this way along the lines $\Gamma$ to (0, $\pi$) and $\Gamma$ to ($-\pi$, 0): there is a broad ($\sim$ 1.4 eV wide) dispersive peak visible for **k**-vectors along the (0, $\pi$) direction in **k**-space while along the ($-\pi$, 0) direction, one finds a weaker structure having negligible dispersion in the binding energy range in which the well-developed, dispersive peaks are situated along the (0, $\pi$) direction.

At first sight, the differences between Figures 3a and 3b are surprising because $Ba_2Cu_3O_4Cl_2$ is tetragonal such that the $\Gamma$ to (0, $\pi$) and $\Gamma$ to ($-\pi$, 0) directions in reciprocal space are symmetrically equivalent. This equivalence does not hold, however, for the matrix element for the photoionization process $\langle \text{i}|\ \mathbf{p}\cdot\mathbf{A}|\text{f}\rangle$ ($\langle$i| and |f$\rangle$ are the initial and final states of the photoionization process, respectively), which contains the relative orientation of the photoelectron momentum vector and the vector potential (and hence the electric field) *via* the operator $\mathbf{p}\cdot\mathbf{A}$. First note that for scans along the $\Gamma$ to (0, $\pi$) and $\Gamma$ to ($-\pi$, 0) directions in **k**-space the plane spanned by the photoelectron momentum vector and the sample surface normal (*i.e.* the emission plane) is a symmetry plane of the Hamiltonian (denoted $M_1$ in Fig. 1). This means that

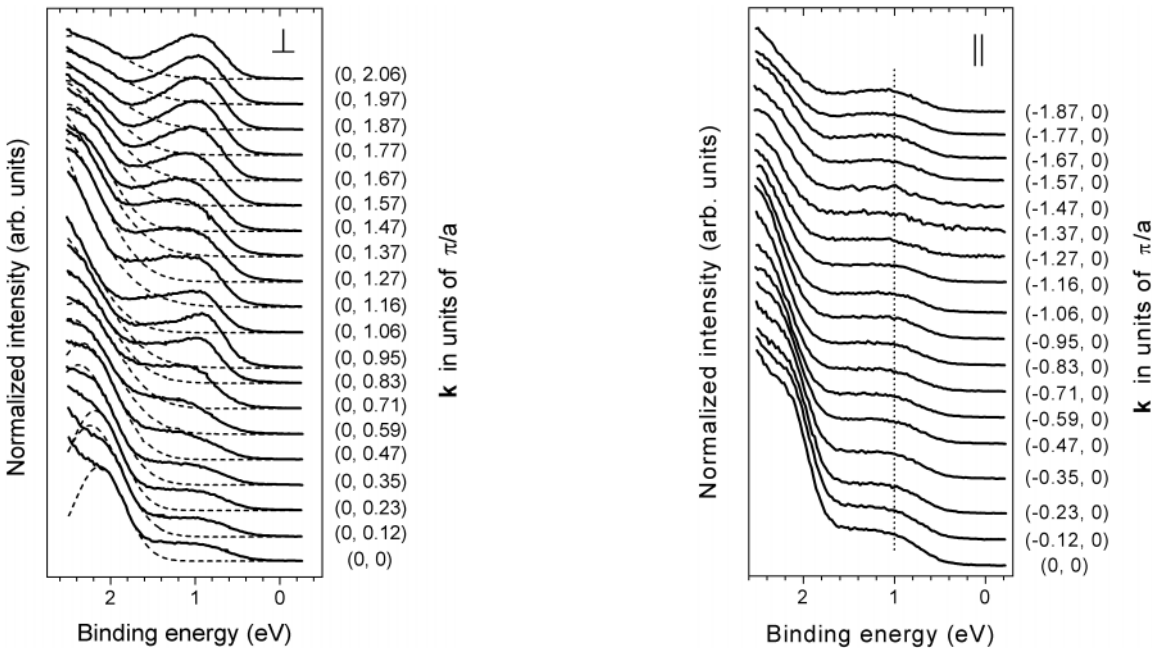


**Fig. 3.** (a) First electron-removal states along $\Gamma$ to $(0, \pi)$ with the electric field vector nearly perpendicular to the emission plane. The dashed lines are the assumed contributions from states at higher binding energies. (b) EDC's along $\Gamma$ to $(-\pi, 0)$ with the electric field vector parallel to the emission plane. The dotted line is a guide to the eyes.

the energy eigenfunctions, and hence $\langle$i| and |f$\rangle$, are also eigenfunctions of the parity operator with respect to the emission plane. Furthermore, in a scan along the line $\Gamma$ to $(0, \pi)$, the electric field vector is nearly perpendicular to the emission plane – which we denote as perpendicular polarization – while in a scan along the line $\Gamma$ to $(-\pi, 0)$, the electric field vector is parallel to the emission plane (parallel polarization) – which corresponds to odd and even parity of the operator $\mathbf{p}\cdot\mathbf{A}$ with respect to the emission plane, respectively. The photoionization matrix element, however, is zero when $\langle$i| and $\mathbf{p}\cdot\mathbf{A}$|f$\rangle$ have different parities with respect to the emission plane. As the dispersing features are observed only for perpendicular polarization of the electric field vector and therefore odd parity of the operator $\mathbf{p}\cdot\mathbf{A}$ with respect to the emission plane, one can conclude that the parities of the initial and final states have to be different with respect to mirror plane $M_1$.

Assuming weakly interacting QP's, further information about the symmetry of the wave function of the lowest lying states can be gained. The photoionization matrix element then reduces to $\langle\phi\,|\,\mathbf{p}\cdot\mathbf{A}\,|\,\varepsilon\rangle$ where $\langle\phi\,|$ is the state from which the photoelectron stems while $|\,\varepsilon\rangle$ is the free electron final state of the photoelectron. $|\,\varepsilon\rangle$ must have even parity with respect to the emission plane, otherwise the wavefunction of the photoelectron would have a node in the emission plane and could not be detected by the analyzer. Thus the matrix element is only non-zero for perpendicular polarization of the electric field vector (odd parity of $\mathbf{p}\cdot\mathbf{A}$) if the initial state has odd parity while for parallel polarization the initial state has to have even parity.

From the observed polarization dependence of the first electron-removal states for **k**-vectors along the $\Gamma$ to $(-\pi, 0)/(0, \pi)$ direction in reciprocal space we can conclude that the initial state has odd parity with respect to mirror plane $M_1$ in Figure 1 which is in agreement with the results for 35 eV photons along the equivalent direction in references [13,14] and with the symmetry of a Zhang-Rice singlet [20] (ZRS).

Figures 4a and 4b present EDC's from $\Gamma$ to $(-\pi, \pi)$ and from $\Gamma$ to $(\pi, \pi)$; the sample was oriented such that the $\Gamma$ to $(\pi, \pi)$ direction in reciprocal space is in the horizontal plane. A broad and dispersive peak spanning a range of nearly 1.4 eV can be seen for both directions with essentially the same relative spectral strength with respect to the main valence band. The $\Gamma$ to $(\pi, \pi)$ and $\Gamma$ to $(-\pi, \pi)$ directions in **k**-space are symmetrically equivalent but differ in the alignment of the electric field vector with respect to the emission plane. In a scan from $\Gamma$ to $(\pi, \pi)$ the electric field vector is always in the emission plane while for a scan from $\Gamma$ to $(-\pi, \pi)$ it is nearly perpendicular to the emission plane. In contrast to the situation for the scans along the lines $\Gamma$ to $(-\pi, 0)$ and $\Gamma$ to $(0, \pi)$, the emission plane is a mirror plane of the geometrical structure of the $Cu_3O_4$ plane, but not a mirror plane of the Hamiltonian if the antiferromagnetic spin order in the $Cu_A$-O subsystem is taken into account (see mirror plane $M_2$ in Fig. 1). Since the QP wavefunction does not

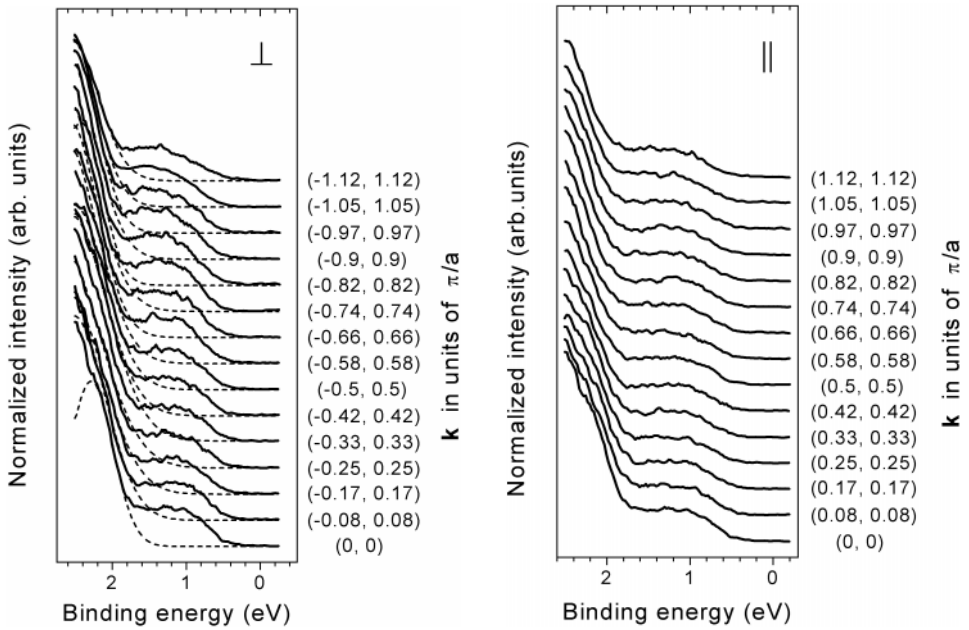


**Fig. 4.** (a) First electron-removal states from $\Gamma$ to $(-\pi, \pi)$ with the electric field vector nearly perpendicular to the emission plane. The dashed lines are the assumed contributions from states at higher binding energies. (b) First electron-removal states from $\Gamma$ to $(\pi, \pi)$ with the electric field vector parallel to the emission plane.

have a definite parity with respect to the emission plane it is reasonable that the feature is visible for both polarizations. A similar polarization dependence of the first electron-removal states along the $\Gamma$ to $(\pi, \pi)$ direction was observed at 35 eV photon energy [14].

EDC's along the edges of the BZ and the antiferromagnetic BZ from $(0, \pi)$ to $(-\pi, \pi)$ and from $(-\pi, 0)$ to $(0, \pi)$ are shown in Figures 5 and 6. The electronic states also have no definite parity with respect to the emission plane for these scans, as in both cases the emission planes are not mirror planes of the $Cu_3O_4$ plane, except at high symmetry points such as $(0, \pi)$. Therefore, the polarization dependence of the first electron-removal states along these lines in **k**-space will not be discussed here.

### 3.3 The first electron-removal states of $Ba_2Cu_3O_4Cl_2$ - lineshape and dispersion

Let us now turn to the dispersion and lineshape of the first electron-removal states of $Ba_2Cu_3O_4Cl_2$. To facilitate the detailed analysis of the first electron-removal states, the contributions from the higher lying states as indicated by the dashed lines in Figures 3–6 can be removed using the procedure already outlined. Figures 7–10 present the first electron-removal states after subtracting the contributions from the main VB for scans from $\Gamma$ to $(0, \pi)$, from $\Gamma$ to $(-\pi, \pi)$ and both along the edge of the BZ and along the edge of the antiferromagnetic BZ.

Inspection of Figures 7–10 reveals that the first electron-removal states of $Ba_2Cu_3O_4Cl_2$ are composed of

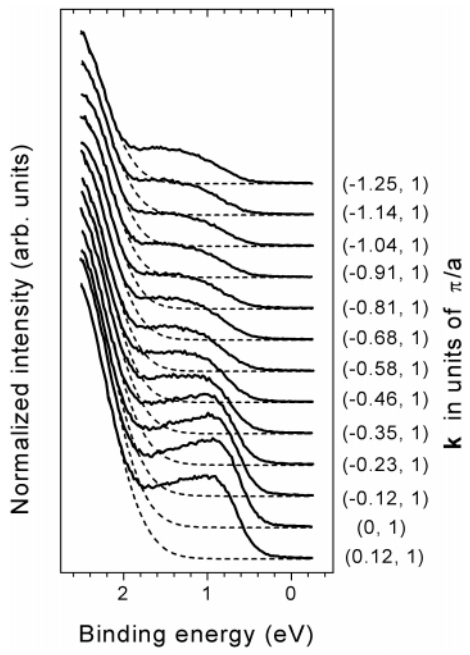


**Fig. 5.** First electron-removal states from $(0, \pi)$ to $(-\pi, \pi)$. The dashed lines are the assumed contributions from states at higher binding energies.

two components as indicated using open and closed circles. In Figure 7 around $(0, \pi)$ a low energy peak at $\sim 0.9$ eV and a shoulder at $\sim 0.5$ eV higher binding energy can be

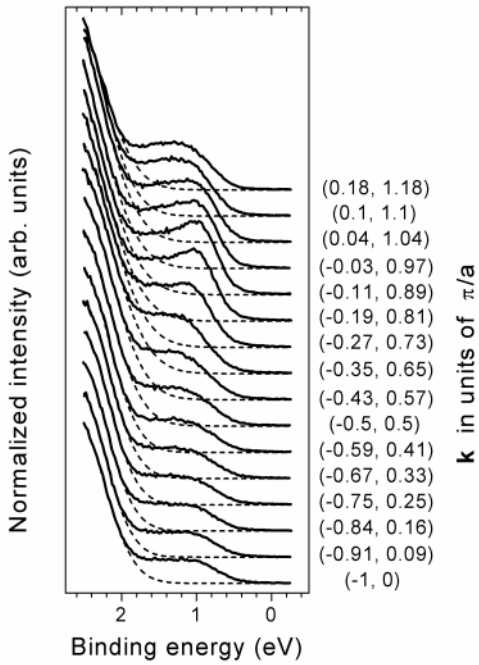


**Fig. 6.** First electron-removal states from $(-\pi, 0)$ to $(0, \pi)$. The dashed lines are the assumed contributions from states at higher binding energies.

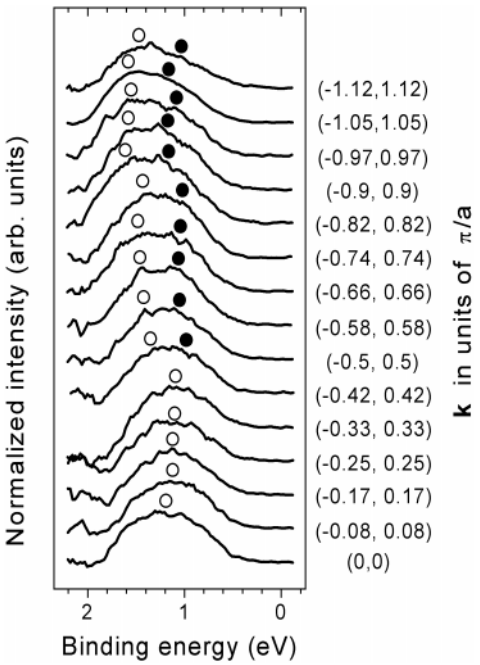


**Fig. 8.** Same as Figure 4a but with the contributions due to higher lying states having been removed.

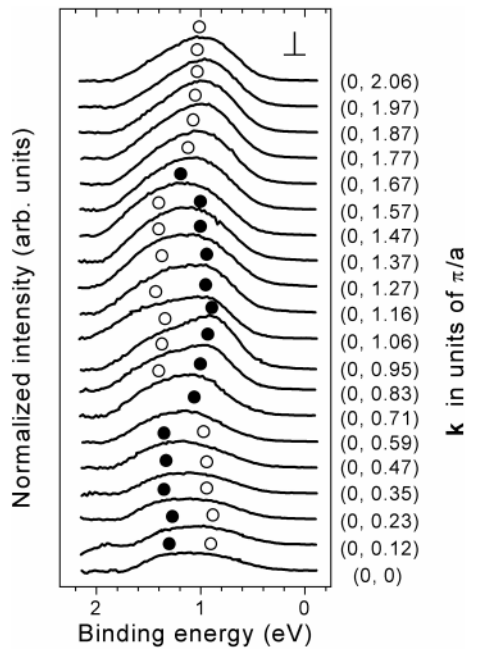


**Fig. 7.** Same as Figure 3a but with the contributions due to higher lying states having been removed.

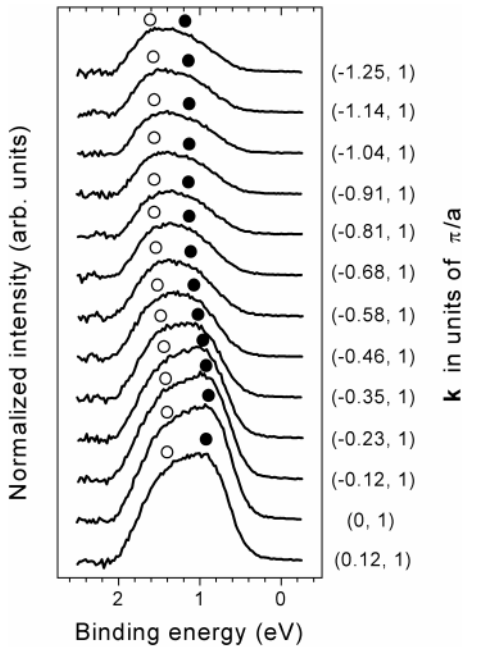


**Fig. 9.** Same as Figure 5 but with the contributions due to higher lying states having been removed.

clearly seen. Furthermore the spectra recorded along the edge of the BZ and along the antiferromagnetic BZ boundary (Figs. 9 and 10) exhibit low and high binding energy components. Under certain experimental conditions only one component is visible as in Figure 7 from $(0, 3/2\pi)$ to $(0, 2\pi)$. The fact that the ARPES spectra in the equivalent **k**-space region from $\Gamma$ to $(0, 1/2\pi)$ are different in lineshape and have much less spectral intensity suggests that matrix element effects are strong in $Ba_2Cu_3O_4Cl_2$. Similar effects have been found previously in cuprate superconductors [21,22].

Insight into the origin of the two compents of the first electron-removal states of $Ba_2Cu_3O_4Cl_2$ can be gained by comparison with $Sr_2CuO_2Cl_2$ ARPES data [9–11].

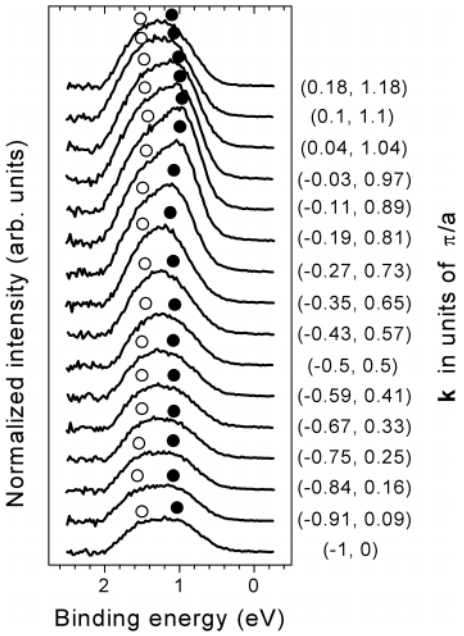


**Fig. 10.** Same as Figure 6 but with contributions due to higher lying states having been removed.

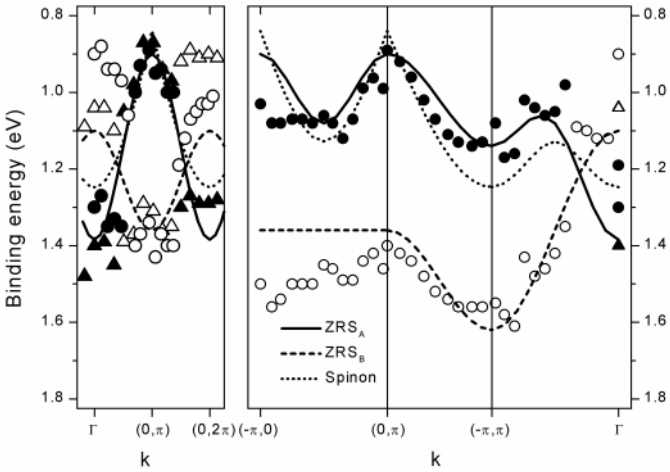


**Fig. 11.** Comparison of dispersion relations determined using ARPES with the best fits of the predicted ZRS dispersion relations for a two-dimensional antiferromagnetic spin background (solid line, Eq. (1)), a paramagnetic spin network (dashed line, Eq. (3)) and the spinon dispersion relation (dotted line, Eq. (2)). The model parameters are given in Table 1. The data points fitted from the ARPES spectra are assigned to belong either to the $Cu_A$-O (solid circles: 20 eV photon energy (this work), solid triangles: 35 eV photon energy (Refs. [13,14])) or the $Cu_B$-O subsystem (open circles: 20 eV photon energy (this work), open triangles: 35 eV photon energy (Refs. [13,14])).

One should note that a $CuO_4$ plaquette of the antiferromagnetically ordered $Cu_A$-O subsystem of $Ba_2Cu_3O_4Cl_2$ (corresponding to the $CuO_4$ unit of the $CuO_2$ plane of $Sr_2CuO_2Cl_2$) is rotated by 45° and has half the area of the $Cu_3O_4$ plane unit cell. Therefore, the ARPES spectra at the $(0, \pi)$ point in $Ba_2Cu_3O_4Cl_2$ should be compared with spectra at the $(\pi/2, \pi/2)$ point of $Sr_2CuO_2Cl_2$. Thus, as in $Sr_2CuO_2Cl_2$ at $(\pi/2, \pi/2)$, the low energy peak observed at $(0, \pi)$ in the $Ba_2Cu_3O_4Cl_2$ ARPES data can be assigned to the photohole in the antiferromagnetically ordered $Cu_A$-O subsystem. For the photon energies used in this work, the first electron-removal states of $Sr_2CuO_2Cl_2$ lack intensity shortly after $(\pi/2, \pi/2)$ on going from $\Gamma$ to $(\pi, \pi)$ and for **k**-vectors from $\Gamma$ to $\sim (\pi/2, 0)$. The strong peak-like structure observed between $(0, 3/2\pi)$ and $(0, 2\pi)$ in $Ba_2Cu_3O_4Cl_2$ cannot then be related to the $Cu_A$-O subsystem, but must be mainly derived from the $Cu_B$-O subsystem. An important consequence of this assignment is that the dispersion of the peak related to the $Cu_B$-O subsystem is different from that expected for the photohole in the $Cu_A$-O subsystem: while the former disperses to lower binding energy on going from $(0, 3/2\pi)$ to $(0, 2\pi)$ one can conclude from the $Sr_2CuO_2Cl_2$ ARPES data that the latter should reach its minimal binding energy at $(0, \pi)$ and then disperse back to higher binding energy on going to $(0, 2\pi)$. These findings suggest that it might be possible to analyze the **k**-dependent energy variations of the two features observed in the first electron-removal states of $Ba_2Cu_3O_4Cl_2$ in terms of the dispersion relations of two different physical objects: one related to the motion of the hole injected by the photoemission process in the antiferromagnetically ordered $Cu_A$-O subsystem while the second is associated with the motion of the photohole in the $Cu_B$-O subsystem, which is in a paramagnetic state at room temperature [8].

In the next section the **k**-dependent energy variation of the features evident in Figures 7–10 is compared with theoretical dispersion relations for the single hole dynamics in the antiferromagnetic or paramagnetic spin background of a $Cu_3O_4$ plane. The experimental dispersion relations of the two features of the first electron-removal states have been determined by fitting the data with two Voigt functions. The ARPES spectra recorded from $\Gamma$ to $(-0.42\pi, 0.42\pi)$ and from $(0, 3/2\pi)$ to $(0, 2\pi)$ using 20 eV photon energy were fitted by only one Voigt peak for reasons outlined earlier in this section [23]. The peak positions from the spectra recorded at 20 eV photon energy and 35 eV photon energy [13] are plotted *versus* momentum in Figure 11. The incoherent spectral intensity was not accounted for in the fitting process as it is neither possible to extract any information about it directly from the $Ba_2Cu_3O_4Cl_2$ ARPES spectra nor are there concrete theoretical results regarding the incoherent part of the spectral function which would help in an evaluation of the dispersion relations.

### 3.4 The first electron-removal states of $Ba_2Cu_3O_4Cl_2$ - comparison with theory

After having taken the plausible step of accepting that the **k**-variation of the peak locations can be related to the dynamics of a single hole injected into the $Cu_A$-O and $Cu_B$-O subsystems of $Ba_2Cu_3O_4Cl_2$, the data will be compared to theoretical results on the single hole dynamics in

**Table 1.** Parameters (in eV) for equations (1), (2) and (3), which give the best agreement with the ARPES spectra shown in Figures 7–10.

| **Two-dimensional antiferromagnetic spin network** | | |
|---|---|---|
| ZRS dispersion relation (Eq. (1)) | | |
| $E_A$ | $J$ | $\lambda$ |
| $0.90 \pm 0.04$ eV | $0.22 \pm 0.03$ eV | $0.06 \pm 0.01$ eV |
| Spinon dispersion relation (Eq. (2)) | | |
| $E_A$ | $J$ | - |
| $0.84 \pm 0.06$ eV | $0.18 \pm 0.03$ eV | - |
| **Two-dimensional paramagnetic spin network** | | |
| ZRS dispersion relation (Eq. (3)) | | |
| $E_B$ | $t_B$ | - |
| $1.36 \pm 0.03$ eV | $-0.13 \pm 0.05$ eV | - |

antiferromagnetic and paramagnetic two-dimensional spin networks. Figure 11 shows the best fits to the experimental data with ZRS dispersion relations for an antiferromagnetic and paramagnetic spin network as well as the spinon dispersion relation. The fit parameter values are presented in Table 1.

Figure 11 shows that there is a reasonable agreement between the **k**-dependent variation of the peak locations of the two components observed in the first electron-removal states of $Ba_2Cu_3O_4Cl_2$ and the ZRS dispersion relations for a two-dimensional antiferromagnetic or paramagnetic spin network while the spinon dispersion cannot be brought into similarly good agreement with the experimental data. The dispersion of the component with lowest binding energy around $(0, \pi)$ and $(0, 3\pi)$ ($(0, 3\pi)$ is not shown in Fig. 11), for example, can then be assigned to the motion of the ZRS in the antiferromagnetically ordered $Cu_A$-O subsystem. The **k**-dependent variation of the location of the second component consisting of the shoulder at the high binding energy flank of the peak at $(0, \pi)$ and the low binding energy component observed around $(0, 2\pi)$ can be related to the motion of the ZRS in the $Cu_B$-O subsystem, which is in a paramagnetic state at room temperature. The experimentally observed dispersions of the low and high binding energy components of the first electron-removal states from $(0, \pi)$ to $(-\pi, 0)/(-\pi, \pi)$ can also be assigned to ZRS's in the $Cu_A$-O and $Cu_B$-O subsystems, respectively. Finally, the feature observed from $\Gamma$ to $(-\pi, \pi)$ seems to be related to ZRS's both in the $Cu_A$-O and in the $Cu_B$-O subsystem for most **k**-vectors.

In the following we will give a more detailed comparison of the experimental data with theory. Especially, it will be shown that the values of the model parameters obtained by fitting to our data are in good agreement with predictions from theory and the results of other experiments.

### 3.4.1 Single hole in two-dimensional antiferromagnetic spin network – ZRS model

The dynamics of a ZRS can be described within the framework of an effective one-band Hamiltonian, the $t - J$ Hamiltonian. Where $t$ is the hopping integral, which describes the hopping of the ZRS on the copper sublattice, and $J$ is an exchange integral which accounts for the influence of the antiferromagnetic correlations. With long-range antiferromagnetic order, the dispersion relation of a ZRS moving in the $Cu_A$-O sublattice of a $Cu_3O_4$ plane can be approximated by [13]

$$E_k = E_A + 0.55J(\cos(k_s) + \cos(k_d))^2 + \lambda(\cos(k_s) - \cos(k_d))^2 \quad (1)$$

where $E_A$ is a parameter which is determined by the $Cu_A$ $3d$ orbital on-site energy and the binding energies of both the ZRS and the magnetic polaron on the $Cu_A$-O sublattice, $J$ is the exchange integral describing the magnetic interaction between the $Cu_A$ sites, and $\lambda$ is a factor which takes into account hopping to second ($t'$) and third ($t''$) nearest neighbors (extended $t - J$ Hamiltonian), $k_{s,d}$ is equal to $a(k_x \pm k_y)$ (a is the lattice constant of the $Cu_3O_4$ plane). The bandwidth is then $W = 2.2J$ and therefore determined by the exchange integral and not the hopping integral.

A good overall agreement between experiment and the calculated ZRS quasiparticle dispersion for an antiferromagnetic background can be achieved if the parameter set given in Table 1 is used. An extended $t - J$ model ($\lambda$ non-zero in Tab. 1) has to be used as the lowest binding energy of the $Cu_A$-O-derived component along $\Gamma$ to $(0, \pi)$ is $\sim 200$ meV lower than that along $\Gamma$ to $(-\pi, \pi)$, which is significant in the context of the accuracy of the experiment. Keeping the uncertainities in the peak locations in mind ($\sim \pm 0.1$ eV), the fitted $J$-value of 220 meV is in acceptable agreement with values obtained from more accurate measurements for the closely related compound $Sr_2Cu_3O_4Cl_2$ ($J = 130$ meV in Ref. [24]) and many other cuprates [25]. Note that the value of $\lambda$ obtained from the fit here ($\lambda = 0.06 \pm 0.01$ eV) is equal within the error bars to those which are obtained if the $Sr_2CuO_2Cl_2$ ARPES data of reference [9] or references [10,11] are fitted to equation (1). It should be noted here that in the case of the $Sr_2CuO_2Cl_2$ ARPES data of, for example, reference [9] the value of $t'$ required to increase the minimal binding energy of the states along $\Gamma$ to $(\pi, 0)$ sufficiently to get close agreement between the experimental data and numerically calculated peak dispersions (*e.g.* $-t' = 2t'' = 0.4t$, $t = 413$ meV (Ref. [26])) is significantly different from that arrived at from the reduction of the three-band Emery model to the single-band $t - J$ model ($-t' = 0.5t'' = 0.08t$, $t = 498$ meV (Ref. [27])), while for $t''$ there is good agreement.

### 3.4.2 Single hole in two-dimensional antiferromagnetic spin network - spin-charge separation

In the case of an antiferromagnetic background, it has been argued [28,29] that the photohole decays into spinons and holons and that the dispersing peak observed in the $Sr_2CuO_2Cl_2$ ARPES spectra at lowest binding energies is not related to a ZRS but a bound spinon-holon pair,

whose **k**-dependent energy variation maps out the spinon dispersion relation [28,29]. The spinon dispersion relation for a $Cu_3O_4$ plane is given by

$$E_{\mathbf{k}} = E_{\mathrm{A}} + 1.6J\sqrt{\cos^2(k_s a) + \cos^2(k_d a)} \qquad (2)$$

using the same notation as in equation(1).

The best fit of the spinon dispersion relation to our experimental data is worse than for the ZRS dispersion relation calculated from an extended $t-J$ model. A further signature for spin-charge separation in the antiferromagnetic $Cu_A$-O subsystem would be a step-like lineshape of the first electron-removal states derived from the $Cu_A$-O network from $\Gamma$ to $(-\pi, \pi)$ [28]. The lineshape of the first electron-removal states of $Ba_2Cu_3O_4Cl_2$ from $\Gamma$ to $(-\pi, \pi)$, however, cannot be used for this purpose because the spectral intensity from the $Cu_A$-O and $Cu_B$-O subsystems overlap (see Fig. 8). Nonetheless, in the $Sr_2CuO_2Cl_2$ ARPES data of references [10,11] and [30] a peak-like feature is observed for **k**-vectors from $\Gamma$ to $(\pi, 0)$ [31] which is in contradiction to the step-like lineshape expected for spin-charge separation [28]. From an analysis of the $Sr_2CuO_2Cl_2$ and the available $Ba_2Cu_3O_4Cl_2$ ARPES data, one can therefore conclude that, in contrast to the situation in an one-dimensional antiferromagnetic chain [32,33], it is rather unlikely that a hole injected into a two-dimensional antiferromagnetic Cu-O plane decays into spinons and holons.

### 3.4.3 Single hole in a two-dimensional paramagnetic spin network - ZRS model

The dispersion relation of a ZRS moving in the paramagnetic $Cu_B$-O subsystem is given by [13]

$$E_k = E_{\mathrm{B}} + t_{\mathrm{B}}(\cos(k_x a) + \cos(k_y a)) \qquad (3)$$

whereby $E_{\mathrm{B}}$ is the $Cu_B$-O sublattice analogon to $E_{\mathrm{A}}$ and $t_{\mathrm{B}}$ is the hopping integral for the ZRS in the $Cu_B$-O subsystem. Here the bandwidth is determined by the hopping integral $t_{\mathrm{B}}$ which is connected to the overlap $t_{pp}^{\perp}$ between mutually perpendicular O $2p$ orbitals on neighbouring oxygen sites of the $Cu_B$-O subsystem (see Fig. 1 of Ref. [13]) according to

$$t_{\mathrm{B}} = -\eta^2 t_{pp}^{\perp}/2. \qquad (4)$$

Taking $\eta = 0.75$ (Ref. [13]) and $t_{pp}^{\perp} = 0.45$ eV from the results of a tight-binding fit to the band-structure of $Ba_2Cu_3O_4Cl_2$ [34], a value of $-0.13$ eV is predicted for $t_{\mathrm{B}}$. The overlap $t_{pp}^{\parallel}$ between mutually parallel O $2p$ orbitals on neighbouring oxygen sites is small [34] and can therefore be neglected.

Regarding the motion of a hole in a paramagnetic background, one has to stress that it is controversial as to whether the calculation leading to equation (3), which makes use of a simple Green's function decoupling scheme using a very limited basis function set and neglects the influence of the distortion of the paramagnetic spin background caused by the movement of the hole ("strings", see *e.g.* Ref. [12]), contains the essential physics of the motion of a hole in a paramagnetic background. In reference [35], the $t-J$ model is analyzed within a generalized string picture including strings of great length to describe the hole motion in a paramagnetic $CuO_2$ plane. A strongly **k**-dependent spectral function results whose lowest energy pole, though not assigned to a QP, also follows a tight-binding-like dispersion

$$E_k = E_{\mathrm{B}} + 1.7t(\cos(k_x a) + \cos(k_y a)) \qquad (5)$$

with $t$ being an effective hopping integral. In the generalized string picture $t$ need not have the same value as the $t_{\mathrm{B}}$ calculated under the assumption of negligible influence of the distortions of the paramagnetic spin background on the hole motion. A bandwidth of $6.8t$ can be defined from the locations of the peak maxima at $\Gamma$ and $(\pi, \pi)$ which is considerably larger than the $4t_{\mathrm{B}}$ obtained from equation (2) but, due to electron correlation effects, is still smaller than the $8t$ bandwidth expected, if the one-electron picture were applicable. In reference [35] no connection between the hopping integral $t$ and tight-binding parameters from a band-structure of $Ba_2Cu_3O_4Cl_2$ is given, but from a comparison of equations (3, 4) and (5) one can at least get an estimate of the value of $t$ for $Ba_2Cu_3O_4Cl_2$ which can be estimated to be $t_{\mathrm{B}}/1.7 = -0.08$ eV for $t_{\mathrm{B}} = -0.13$ eV.

Figure 11 shows that the dispersion of one component of the first electron-removal states of $Ba_2Cu_3O_4Cl_2$ can be described in an approximative manner by a tight-binding dispersion relation. The fitted value for the parameter $t_{\mathrm{B}}$ (see Tab. 1) is in perfect agreement with the $-0.13$ eV predicted from theory (Eq. (4)).

It should be noted that the $Cu_B$-related first electron-removal states in $Ba_2Cu_3O_4Cl_2$ are twice as broad (typically 1.4–1.8 eV, see *e.g.* spectra from $(0, 3/2\pi)$ to $(0, 2\pi)$ in Fig. 7) as the low energy peak observed in the first electron-removal states related to the motion of the photohole in an antiferromagnetically ordered Cu-O network at similar temperatures [9,10]. There are no indications that this is related to an experimental artefact: a broadening of the first electron-removal states of $Ba_2Cu_3O_4Cl_2$ due to charging effects can be excluded. It is possible that the widths of the first electron-removal states are not representative of the inverse lifetime of the hole, however, such drastic effects have only been observed in special cases [36]. Thus the large width of the $Cu_B$-derived peak in the first electron-removal states of $Ba_2Cu_3O_4Cl_2$ seems to be intrinsic and related to the spectral function.

The question remains which processes are responsible for the comparatively short lifetime of the photohole in the $Cu_B$-O subsystem. String excitations are one possibility, so it is interesting to compare the spectral function calculated using the two-dimensional $t-J$ model in the generalized string picture with the $Cu_B$-derived part of the spectral intensity. In Figure 12 the results of reference [35] at the $\Gamma$ point and $(\pi/2, \pi/2)$ have been replotted after broadening with a Gaussian, full width at half maximum = 150 meV, to account for the experimental energy resolution.

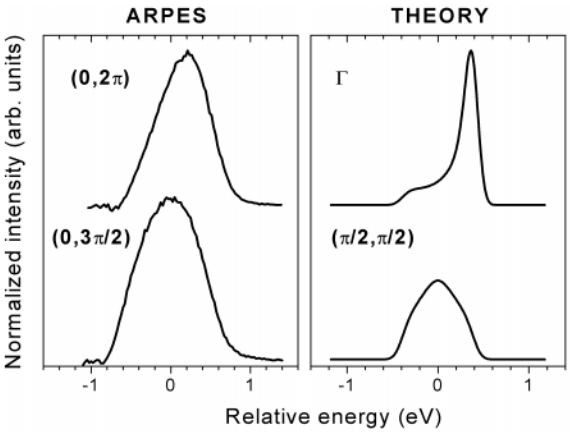


**Fig. 12.** Comparison between the calculated one-hole spectral function for a two-dimensional paramagnetic spin background (right panel) and the first electron-removal states of $Ba_2Cu_3O_4Cl_2$ (left panel). Note that the **k**-labels of the experimental/theoretical curves are given with respect to the first BZ of a $Cu_3O_4/CuO_2$ plane, respectively. See the text for further details.

In reference [35], the spectral function was calculated for a paramagnetic $CuO_2$ plane – when comparing with the first electron-removal states derived from the $Cu_B$-O subsystem of $Ba_2Cu_3O_4Cl_2$ one should note that $(\pi, \pi)$ in the BZ derived from the repeat unit of the $Cu_B$-O subsystem alone corresponds to $(0, \pi)$ in the BZ of the $Cu_3O_4$ plane [37]. This means that the first electron-removal states at $(0, 2\pi)$ and $(0, 3/2\pi)$ (with respect to the BZ of the $Cu_3O_4$ plane) have to be compared with the calculated spectral functions at $\Gamma$ and $(\pi/2, \pi/2)$ (with respect to the BZ of a $CuO_2$ plane) as in Figure 12. It is evident that the calculated spectral functions do not reproduce the widths of the corresponding first electron-removal states. String excitations alone are therefore insufficient to explain the relatively short lifetimes of the holes injected into the paramagnetic $Cu_B$-O subsystem. Further experimental and theoretical work will be necessary to clarify this question.

## 4 Conclusions

The first electron-removal states of the layered cuprate $Ba_2Cu_3O_4Cl_2$ have been measured using polarization dependent angle-resolved photoelectron spectroscopy along the lines $\Gamma$ to $(0, \pi)$ and $\Gamma$ to $(\pm\pi, \pi)$ and along the edges of the Brillouin zone ($(0, \pi)$ to $(-\pi, \pi)$) and antiferromagnetic Brillouin zone ($(-\pi, 0)$ to $(0, \pi)$) at room temperature. The following conclusions regarding the physics of the motion of a single hole in a two-dimensional antiferromagnetic or paramagnetic Cu-O network can be drawn:

(a) The first electron-removal states show two dispersive features which can be assigned in a reasonable way to the motion of the injected photohole in the antiferromagnetic $Cu_A$-O and the paramagnetic $Cu_B$-O subsystem, respectively.

(b) The first electron-removal states have odd parity with respect to mirror plane $M_1$ of the geometrical structure of the $Cu_3O_4$ plane (see Fig. 1) which is compatible with the symmetry expected for a Zhang-Rice singlet.

(c) The spinon dispersion relation is in worse agreement with the experimentally observed dispersion relation of the first electron-removal states related to the photohole in the $Cu_A$-O subsystem than the ZRS dispersion. This and the lineshape of the first electron-removal states of $Sr_2CuO_2Cl_2$ from $\Gamma$ to $(\pi, 0)$ shown in references [10,11,30] indicate that a hole injected into a two-dimensional antiferromagnetically ordered Cu-O network does not decay into spinons and holons.

(d) The motion of a single hole in the antiferromagnetically ordered $Cu_A$-O subsystem can be described within a one-band model including extra hopping terms (extended $t - J$ model). The values obtained for the parameters are in reasonable agreement to those arrived at from the $Sr_2CuO_2Cl_2$ ARPES data of references [9–11]. In general, a $t'$ and $t''$ as required to fit the results of band-structure calculations [38], and a reduction of the three-band model using the generally accepted cuprate parameters also landed in the extended $t - J$ regime [27].

(e) The **k**-dependent energy variation of the feature related to the photohole in the $Cu_B$-O subsystem is governed by a hopping matrix element and can be described by a tight-binding dispersion relation with a bandwidth which is significantly smaller than that of independent electrons due to electron correlation effects. The photohole formed in the paramagnetic $Cu_B$-O subsystem has a short lifetime when compared to that of the analogous excitation in the antiferromagnetic $Cu_A$-O subsystem. It is not clear which processes can account for the relatively short lifetime of the hole injected into the paramagnetic $Cu_B$-O subsystem. String excitations alone cannot account for the widths of the first electron-removal states of the $Cu_B$-O subsystem.

This work was funded by the BMBF under project No. 05605 BDA and 05605 GUA. S.H. acknowledges the DFG for support within the framework of the *Graduiertenkolleg "Struktur und Korrelationseffekte in Festkörpern" der TU Dresden*, S.R.K. acknowledges SFB 463 for support. We are grateful to W. Höppner for technical assistance, H. Zhang, D. Schläfer and A. Theresiak for carrying out the crystal orientation and to H. Rosner, R. Hayn, M. Vojta and K.W. Becker for helpful discussions.

## References


1. G. Mante, *et al.*, Z. Phys. B **80**, 181 (1990); C.G. Olson, *et al.*, Phys. Rev. B **420**, 381 (1990); J.C. Campuzano, *et al.*, Phys. Rev. Lett. **64**, 2308 (1990); D.M. King, *et al.*, *ibid.* **70**, 3159 (1993); R.O. Anderson, *et al.*, *ibid.* **70**, 3163 (1993).
2. Z.-X. Shen, *et al.*, Phys. Rev. Lett. **70**, 1553 (1993); H. Ding, *et al.*, *ibid.* **74**, 2784 (1995).
3. D.S. Marshall, *et al.*, Phys. Rev. Lett **76**, 4841 (1996); H. Ding, *et al.*, Nature **382**, 51 (1996); A.G. Loeser, *et al.*, Science **273**, 325 (1996).
4. A. Ino, *et al.*, J. Phys. Soc. Jpn **68**, 1496 (1999).
5. S. Haffner, *et al.*, Phys. Rev. B **57**, 3672 (1998).
6. D. Vaknin, *et al.*, Phys. Rev. B **41**, 1926 (1990).
7. S. Noro, H. Suzuki, T. Yamadaya, Solid State Commun. **76**, 711 (1990); S. Noro, *et al.*, Mater. Sci. Eng. B **25**, 167 (1994).
8. K. Yamada, N. Suzuki, J. Akimitsu, Physica B **213/214**, 191 (1995).
9. B.O. Wells, *et al.*, Phys. Rev. Lett. **74**, 964 (1995).
10. S. LaRosa, *et al.*, Phys. Rev. B **56**, 525 (1997).
11. C. Kim, *et al.*, Phys. Rev. Lett. **80**, 4245 (1998).
12. E. Dagotto, Rev. Mod. Phys. **66**, 763 (1994).
13. M.S. Golden, *et al.*, Phys. Rev. Lett. **78**, 4107 (1997).
14. H.C. Schmelz, *et al.*, Phys. Rev. B **57**, 10936 (1998).
15. Locations in **k**-space are given in units of the inverse lattice constant of the $Cu_3O_4$ plane.
16. S. Hüfner, *Photoelectron Spectroscopy* (Springer Verlag, Berlin 1995).
17. W. Nolting, *Viel-Teilchen-Theorie* (Zimmermann Verlag, Ulmen 1995).
18. P.W. Leung, B.O. Wells, R.J. Gooding, Phys. Rev. B **56**, 6320 (1997).
19. R. Claessen, *et al.*, Phys. Rev. B **54**, 2453 (1996); T. Yokoya, *et al.*, *ibid.* **54**, 13311 (1996).
20. F.C. Zhang, T.M. Rice, Phys. Rev. B **37**, 3759 (1988).
21. J.G. Tobin, *et al.*, Phys. Rev. B **45**, 5563 (1992).
22. C.G. Olson, *et al.*, J. Phys. Chem. Solids **56**, 1879 (1995).
23. The first electron-removal states recorded at 35 eV photon energy for **k** vectors from $(\pi, 0)$ to $(2\pi, 0)$ (from Ref. [13]) are fitted with two Voigt functions as the overall spectral intensity of the first electron-removal is so low that one cannot exclude a significant contribution from the antiferromagnetically ordered $Cu_A$-O subsystem to it.
24. F.C. Chou, *et al.*, Phys. Rev. Lett. **78**, 535 (1997).
25. Y. Tokura, *et al.*, Phys. Rev. B **41**, 11657 (1990).
26. B. Kyung, R.A. Ferrell, Phys. Rev. B **54**, 10125 (1996).
27. V. Yu. Yushankhai, V.S. Oudovenko, R. Hayn, Phys. Rev. B **55**, 15562 (1997).
28. R.B. Laughlin, J. Phys. Chem. Solids **56**, 1627 (1995).
29. R.B. Laughlin, Phys. Rev. Lett. **79**, 1726 (1997).
30. S. Haffner, Ph.D. thesis, TU Dresden (1998).
31. The $\Gamma-(\pi, 0)$ direction in $Sr_2CuO_2Cl_2$ corresponds to the $\Gamma-(\pi, \pi)$ direction in $Ba_2Cu_3O_4Cl_2$ and *vice versa*, as the unit cells are rotated by 45° with respect to each other.
32. C. Kim, *et al.*, Phys. Rev. Lett. **77**, 4054 (1996).
33. H. Fujisawa, *et al.*, Solid State Commun. **106**, 543 (1998).
34. H. Rosner, R. Hayn, J. Schulenberg, Phys. Rev. B **57**, 13660 (1998).
35. M. Vojta, K.W. Becker, Phys. Rev. B **57**, 3099 (1998).
36. E.D. Hansen, T. Miller, T.-C. Chiang, Phys. Rev. Lett. **80**, 1766 (1998).
37. The minimal real space repeat unit of the $Cu_B$-O subsystem has double the area of the unit cell of the $Cu_3O_4$ plane and is rotated at an angle of 45° with respect to it. Thus the $(\pi, \pi)$ point of the BZ resulting from the $Cu_B$-O repeat unit alone corresponds to the $(\pi, 0)$ point of the regular $Cu_3O_4$ BZ.
38. R. Hayn (private communication).